

填表说明

一、本报告中相关的技术或数据如涉及知识产权保护、军工项目保密等内容，请作脱密处理。

二、请用宋体小四字号撰写本报告，可另行附页或增加页数，A4纸双面打印。

三、表中所涉及的签名都必须用蓝、黑色墨水笔，亲笔签名或签字章，不可以打印代替。

四、同行专家业内评价意见书编号由工程师学院填写，编号规则为：年份4位+申报工程师职称专业类别(领域)4位+流水号3位，共11位。

一、个人申报

(一) 基本情况【围绕《浙江工程师学院（浙江大学工程师学院）工程类专业学位研究生工程师职称评审参考指标》，结合该专业类别(领域)工程师职称评审相关标准，举例说明】

1. 对本专业基础理论知识和专业技术知识掌握情况(不少于200字)

在本专业的基础理论知识和专业技术知识方面，我通过系统学习和深入研究，掌握了扎实的理论基础和前沿技术应用。首先，我通过阅读大量国内外文献，深入了解了磁共振成像（MRI）在医学诊断中的广泛应用，特别是其在不同磁场强度下的成像原理及安全性问题。我重点研究了射频感应加热（RF heating）这一核心问题，认识到其在MRI技术中的重要性及其对患者安全的潜在影响。为了深入理解这一问题，我系统学习了电磁场与热场的相互作用机制，并掌握了电磁场与热场的联合仿真技术，如有限元法（FEM）和时域有限差分法（FDTD）。这些仿真技术为我后续的实验设计和数据分析提供了坚实的理论基础，使我能够从理论层面预测和优化MRI设备的安全性。此外，我还关注了MRI技术的最新发展动态，包括高场强MRI的技术挑战及其解决方案，例如射频屏蔽技术和新型线圈设计。通过理论与实践的结合，我不仅加深了对MRI技术的理解，还具备了解决实际工程问题的能力。未来，我将继续关注本领域的前沿进展，进一步提升自己的专业水平，为医学影像技术的发展贡献力量。

2. 工程实践的经历(不少于200字)

我深入参与了人工耳蜗植入体在MRI环境下的热效应评价方法与装置的研究工作，积累了丰富的工程实践经验。首先，在数值仿真层面，我使用COMSOL多物理场仿真软件建立了鸟笼线圈和人工耳蜗植入体的3D模型，并通过有限元法（FEM）对不同磁场强度（如1.5T和3T）下的射频感应加热效应进行了电磁场仿真分析。在此基础上，我进一步计算了比吸收率（SAR），并将其作为热仿真的输入，利用COMSOL的传热模块求解热传导方程，得到了温度场分布，确定了最恶劣情况构型和最大温升位置。在物理试验阶段，我参与了符合ASTM标准的盐水凝胶体模的制备，并将人工耳蜗植入体放置在体模中，使用MRI系统进行照射实验。通过光纤温度测量探针，我记录了温升数据，并与仿真结果进行了对比分析。此外，我还计算了CE M43结果，以量化人工耳蜗在MRI环境下的热效应安全性。整个研究过程中，我不仅掌握了电磁场与热场的联合仿真技术，还熟悉了物理试验的设计与实施流程，积累了从理论到实践的全链条工程经验。这些实践经历极大地提升了我的问题解决能力和工程实践水平，为未来从事相关领域的研究与开发工作奠定了坚实基础。

3. 在实际工作中综合运用所学知识解决复杂工程问题的案例（不少于1000字）

在进行“人工耳蜗植入体的MRI下热效应评价方法与装置研究”这一课题的专业实践中，我取得了显著的成效，不仅体现在技术应用创新、成果转化及解决企业工程实际问题，还紧密关联了我的学位论文撰写。以下将详细阐述这些方面的收获。

1. 技术应用创新与成果转化

在技术应用创新方面，我深入研究了人工耳蜗植入体在MRI扫描过程中的射频感应加热问题，提出了一种基于数值仿真和物理试验相结合的综合评价方法。通过有限元方法（FEM）对鸟笼线圈及人工耳蜗植入体进行精确的电磁和热联合仿真，我成功确定了最恶劣情况下的加热构型和最大温升位置。这一技术创新不仅提高了评估的准确性和效率，还为后续的物理试验提供了可靠的参考。

在成果转化方面，我所研究的评估方法和装置具有广阔的应用前景。首先，该方法可以直接应用于人工耳蜗植入体在MRI扫描中的安全性评估，为医疗机构提供可靠的技术支持。其次，该方法可以推广到其他有源植入体的MRI安全性评估中，如心脏起搏器、神经刺激器等，

为这些植入设备的安全性研究提供新的思路和工具。通过与相关医疗器械企业合作，该技术有望转化为实际产品，为医疗行业带来显著的经济和社会效益。

2. 解决企业工程实际问题

在解决企业工程实际问题方面，我的研究成果为相关医疗器械企业提供了重要的技术支持。通过与企业合作，我们针对特定型号的人工耳蜗植入体进行了详细的MRI下热效应评估，并为企业提供了针对性的改进建议。这些建议包括优化植入体的设计、改进植入位置以及制定更加合理的MRI扫描方案等，有效降低了植入体在MRI扫描中的射频感应加热风险，提高了患者的安全性。同时，该研究成果也为企业节省了大量的研发成本和试验时间，提升了企业的市场竞争力。

3. 综合运用所学知识解决复杂工程问题的案例

在实际工作中，我综合运用了所学的电磁场理论、热传导理论、数值仿真技术和实验设计方法，成功解决了人工耳蜗植入体在MRI环境下的热效应评估问题。以下是我在解决这一复杂工程问题中的具体实践案例：

3.1 问题分析与需求定义

首先，我与团队成员一起对人工耳蜗植入体在MRI环境下的热效应问题进行了深入分析。我们发现，射频感应加热是导致植入体温度升高的主要原因，而温度过高可能对患者造成伤害。因此，我们需要开发一种能够准确评估植入体在MRI扫描过程中温升的方法和装置。

3.2 数值仿真与模型建立

为了准确评估植入体的温升情况，我使用COMSOL多物理场仿真软件建立了鸟笼线圈和人工耳蜗植入体的3D模型。通过有限元方法（FEM），我对不同磁场强度（如1.5T和3T）下的射频感应加热效应进行了电磁场仿真分析。在此基础上，我进一步计算了比吸收率（SAR），并将其作为热仿真的输入，利用COMSOL的传热模块求解热传导方程，得到了温度场分布，确定了最恶劣情况构型和最大温升位置。

3.3 物理试验设计与实施

为了验证仿真结果的准确性，我参与了符合ASTM标准的盐水凝胶体模的制备，并将人工耳蜗植入体放置在体模中，使用MRI系统进行照射实验。通过光纤温度测量探针，我记录了温升数据，并与仿真结果进行了对比分析。这一过程不仅验证了仿真模型的可靠性，还为后续的优化设计提供了实验依据。

3.4 数据分析与结果评估

在获得仿真和实验数据后，我对数据进行了详细的分析和评估。通过对比仿真结果与实验数据，我发现两者具有较高的一致性，证明了仿真模型的准确性。此外，我还计算了CEM43结果，以量化人工耳蜗在MRI环境下的热效应安全性。这些分析结果为制定更加合理的MRI扫描方案提供了科学依据。

3.5 优化设计与改进建议

基于仿真和实验结果，我为相关医疗器械企业提供了针对性的改进建议。这些建议包括优化植入体的设计、改进植入位置以及制定更加合理的MRI扫描方案等。通过这些改进措施，我们有效降低了植入体在MRI扫描中的射频感应加热风险，提高了患者的安全性。

3.6 成果转化与应用推广

在完成技术研究和优化设计后，我与相关医疗器械企业合作，将研究成果转化为实际产品。通过与企业合作，我们成功开发了一种用于评估人工耳蜗植入体在MRI环境下热效应的装置，并申请了相关专利。该装置不仅能够准确评估植入体的温升情况，还可以推广到其他有源植入体的MRI安全性评估中，为医疗行业带来了显著的经济和社会效益。

4. 总结与展望

通过本次课题研究，我不仅掌握了电磁场与热场的联合仿真技术，还熟悉了物理试验的设计与实施流程，积累了从理论到实践的全链条工程经验。这些实践经历极大地提升了我的问题

解决能力和工程实践水平，为未来从事相关领域的研究与开发工作奠定了坚实基础。未来，我将继续关注本领域的前沿进展，进一步提升自己的专业水平，为医学影像技术的发展贡献力量。

(二) 取得的业绩(代表作)【限填3项, 须提交证明原件(包括发表的论文、出版的著作、专利证书、获奖证书、科技项目立项文件或合同、企业证明等)供核实, 并提供复印件一份】

1. 公开成果代表作【论文发表、专利成果、软件著作权、标准规范与行业工法制定、著作编写、科技成果获奖、学位论文等】

成果名称	成果类别 [含论文、授权专利(含发明专利申请)、软件著作权、标准、工法、著作、获奖、学位论文等]	发表时间/授权或申请时间等	刊物名称/专利授权或申请号等	本人排名/总人数	备注
Simulation and evaluation of thermal effects under MRI for cochlear implants	会议论文	2025年02月25日	18th INTERNATIONAL CONFERENCE ON BIO-INSPIRED SYSTEMS AND SIGNAL PROCESSING	1/5	

2. 其他代表作【主持或参与的课题研究项目、科技成果应用转化推广、企业技术难题解决方案、自主研发设计的产品或样机、技术报告、设计图纸、软课题研究报告、可行性研究报告、规划设计方案、施工或调试报告、工程实验、技术培训教材、推动行业发展中发挥的作用及取得的经济社会效益等】

(三) 在校期间课程、专业实践训练及学位论文相关情况	
课程成绩情况	按课程学分核算的平均成绩： 89 分
专业实践训练时间及考核情况(具有三年及以上工作经历的不作要求)	累计时间： 1 年(要求1年及以上) 考核成绩： 81 分
本人承诺	
<p>个人声明：本人上述所填资料均为真实有效，如有虚假，愿承担一切责任，特此声明！</p> <p style="text-align: right;">申报人签名： 马源佳</p>	

浙江大学研究生院
攻读硕士学位研究生成绩表

学号: 22260305	姓名: 马源伶	性别: 女	学院: 工程师学院	专业: 电子信息	学制: 2.5年						
毕业时最低应获: 24.0学分		已获得: 26.0学分		入学年月: 2022-09	毕业年月:						
学位证书号:			毕业证书号:		授予学位:						
学习时间	课程名称	备注	学分	成绩	课程性质	学习时间	课程名称	备注	学分	成绩	课程性质
2022-2023学年秋季学期	数值计算方法		2.0	94	专业选修课	2022-2023学年春季学期	自然辩证法概论		1.0	91	专业学位课
2022-2023学年秋季学期	现代信号处理技术与应用		1.0	88	专业学位课	2022-2023学年春季学期	智能医疗技术应用案例分析		1.0	98	专业学位课
2022-2023学年秋季学期	工程技术创新前沿		1.5	80	专业学位课	2022-2023学年夏季学期	微纳传感与检测技术导论		2.0	83	专业选修课
2022-2023学年冬季学期	智能化仪器软硬件系统设计与应用		1.0	90	专业学位课	2022-2023学年夏季学期	“四史”专题		1.0	94	公共选修课
2022-2023学年冬季学期	生物医学工程方法学		1.0	87	专业学位课	2023-2024学年冬季学期	工程伦理		2.0	96	专业学位课
2022-2023学年秋冬学期	高阶工程认知实践		3.0	78	专业学位课	2023-2024学年夏季学期	研究生英语应用能力提升		2.0	83	公共学位课
2022-2023学年冬季学期	新时代中国特色社会主义思想理论与实践		2.0	91	专业学位课	2024-2025学年春季学期	跨文化沟通 I		1.0	86	公共学位课
2022-2023学年冬季学期	产业技术发展前沿		1.5	95	专业学位课		硕士生读书报告		2.0	通过	
2022-2023学年秋冬学期	研究生论文写作指导		1.0	90	专业选修课						

说明: 1. 研究生课程按三种方法计分: 百分制, 两级制 (通过、不通过), 五级制 (优、良、中、及格、不及格)。
2. 备注中“*”表示重修课程。

学院成绩校核章:

成绩校核人: 张梦依

打印日期: 2025-03-20



BIODEVICES 2025

18th International Conference on Biomedical Electronics and Devices

<https://biodevices.scitevents.org>

To whom it may concern,

We are happy to inform that the paper submitted by Congcong Zhou to BIODEVICES 2025 with number 58, entitled "Simulation and evaluation of thermal effects under MRI for cochlear implants", has been accepted as a Short Paper, to be presented in Porto - Portugal, February 20 to 22, 2025.

All papers accepted to BIODEVICES 2025 were peer reviewed by at least two experts from the international program committee, in a double-blind review process.

The paper will be published in the conference proceedings with up to 8 pages, and after being presented at BIODEVICES 2025 it will be included in the SCITEPRESS Digital Library under a specific DOI to be specified after the proceedings are published, and submitted for indexation to SCOPUS, Google Scholar, DBLP, Semantic Scholar, EI and Web of Science / Conference Proceedings Citation Index.

Best Regards,

A handwritten signature in black ink, appearing to read "Hugo Gamboa".

Hugo Gamboa
(BIOSTEC Conference Co-chair)

Simulation and evaluation of thermal effects under MRI for cochlear implants

Yuanling Ma¹, Dian Yang², Liping Qin³, Xuesong Ye⁴^a and Congcong Zhou⁵^b

¹Biosensor National Special Laboratory, Key Laboratory of Biomedical Engineering of Ministry of Education, College of Biomedical Engineering and Instrument Science, Zhejiang University, Hangzhou, 310027, China

²Zhe Jiang Key Laboratory of Intelligent Rehabilitation and Translational Neuroelectronics

³Zhejiang Institute of Medical Device Supervision and Testing

⁴National Engineering Research Center for Innovation And Application of Minimally Invasive Instruments, College of Biomedical Engineering and Instrument Science, Zhejiang University, Hangzhou, 310027, China

⁵National Engineering Research Center for Innovation And Application of Minimally Invasive Instruments, Sir Run Run Shaw Hospital, School of Medicine, Zhejiang University

Correspondence: zjdxzcc@zju.edu.cn

Keywords: RF-induced heating, Finite Element Method, Cochlear, Electromagnetic safety.

Abstract: Cochlear implantation is a widely used rehabilitation method for severe sensorineural deafness, but MRI scans can induce RF heating in implants, posing safety risks to patients. In this study, a novel finite-element-based electromagnetic and thermal coupled simulation method to obtain the temperature distribution and maximum temperature rise due to RF-induced heating is studied. This method allows for a quick analysis of the worst-case implant configurations and an evaluation of RF heating effects. Additionally, for cochlear implants, we propose a refined model parameters setting method which using a localized cochlear phantom in simulations to analyse key factors affecting RF-induced heating include electrode length, lead trajectory, and phantom model. In this paper, RF heating was evaluated using two phantoms, three electrode lengths, and three typical lead trajectories, with the highest temperature rise observed at 1.922°C in the cochlear phantom. The results show that small variations in electrode length have less impact compared to wire trajectory and phantom model, indicating the need for greater focus on these factors when assessing RF heating in active implants.

1 INTRODUCTION

Deafness is one of the most prevalent disabling conditions worldwide. The World Health Organization (WHO) estimates that hearing impairment costs the global economy approximately \$750 billion annually. Among the primary causes of deafness is severe to profound hearing impairment, which leads to disabling hearing loss (Chadha et al., 2021). For patients with severe or profound sensorineural deafness, cochlear implantation remains the only effective method of rehabilitation (Buchman et al., 2020). The increasing necessity for MRI in cochlear implant users demands rigorous safety assessments (Alberalar et al., 2023), with RF-induced heating being a pivotal area of focus.

Magnetic resonance imaging (MRI) is a widely used diagnostic tool in clinical practice due to its numerous advantages. It is non-invasive, free of ionizing radiation, and can visualize internal structures like the heart and blood vessels without the use of contrast agents. MRI also offers high-resolution imaging of soft tissues, minimal interference from bone artifacts, and multidirectional and multiparametric imaging capabilities (Koptuyug et al., 2023). However, the increasing strength of MRI magnetic fields, combined with the advancement of new MRI technologies, has raised concerns regarding the biological effects and safety of MRI, particularly for patients with medical implants. The high-power radiofrequency (RF) coils used in MRI systems can induce electromagnetic resonance in conductive implants, leading to RF-induced heating, which may

^a <https://orcid.org/0000-0002-3439-3733>

^b <https://orcid.org/0000-0001-8397-1491>

cause irreversible tissue damage, such as burns. This is especially concerning for patients with implants located near sensitive areas, like the brain(Rezai et al., 2002). Cochlear implants, positioned subcutaneously behind the ear and close to the brain, are particularly susceptible to this risk, making RF-induced heating a critical safety issue that requires thorough testing.

Previous studies primarily focused on in vivo testing, a method involving the implantation of devices into animals or human subjects, followed by the monitoring of physiological parameters in an MRI environment. Crane et al. conducted a retrospective analysis of the safety and diagnostic validity of cochlear implants in patients undergoing MRI scans(Crane et al., 2010). However, their study was limited by the absence of quantitative measurements and a lengthy experimental timeline. Additionally, Luechinger et al. evaluated the RF safety of cochlear implants in experimental pigs (Long White breed), while Roger et al. assessed the radiofrequency safety of pacemaker leads in Danish Long White pigs(Luechinger et al., 2005). Despite these efforts, the in vivo approach was constrained by the limitations of measuring locations and difficulties in obtaining precise data.

To ensure standardization, avoid potential medical ethical issues, and improve experimental convenience, the ASTM F2182 standard outlines a test procedure in which the implant is embedded in a gelatinized saline-filled body phantom, exposed to an RF field with a whole-body average specific absorption rate (SAR) of 2 W/kg using a benchtop system. The temperature is monitored for 15 minutes, and the local SAR is determined using a calorimetric method(ASTM International, 2019). Yang et al. found that, for devices implanted in or near bone tissue, the assessment of RF-EMF energy deposition using an ASTM model that incorporates bone provided a better correlation with human models compared to the standard ASTM model(Yang et al., 2024). However, despite the widespread use and study of in vitro body models for RF heating evaluations, significant limitations remain. The human body is a complex, heterogeneous environment composed of various tissues, and the homogeneous gel-saline models used cannot sufficiently mimic the diverse properties of human tissues to accurately reflect the heating effects of implants in such a complex biological environment(Ran et al., 2017).

The ISO/TS 10974:2018 standard outlines a four-layer test methodology designed to account for the wide range of configurations and applications of active implantable medical devices (AIMDs), aiming

to provide a conservative estimate of energy deposition in controlled in vitro test systems (Standardization, 2018). Numerous studies have also employed the Finite-Difference Time-Domain (FDTD) method and transfer function approach to assess RF-induced heating. For example, Zeng et al. evaluated RF heating in a cochlear implant within a 1.5T MRI coil using the FDTD method, alongside a virtual human body model for electromagnetic simulation, and employed the transfer function approach to estimate temperature rise. They also explored variables such as lead type, trajectory, and MRI parameters on RF heating effects(Zeng et al., 2018). Similarly, Islam et al. investigated RF-induced heating in partially inserted electrodes in 1.5T MRI systems, revealing that heating was significantly influenced by factors such as contact size, spacing, lead length, and clinically relevant trajectories(Islam et al., 2023). While this approach has become widely adopted due to its ability to maintain the complexity of the implant system's microstructure, it has some limitations. The accuracy of FDTD EM simulations is moderate, and the measurement of transfer functions requires physical prototypes, making repeated testing time-consuming and less suitable for implants with complex and variable wire geometries, such as cochlear implants. In such cases, alternative methodologies may offer better efficiency and precision(Winter et al., 2021).

The assessment of RF-EMF safety requires consideration of curved components such as birdcage coils and implant electrodes. In this context, the Finite Element Method (FEM) emerges as an optimal approach, offering enhanced precision in analyzing complex, curved geometries compared to other techniques(Winter et al., 2021). This paper introduces a combined electromagnetic and temperature field simulation method, based on the FEM approach, to evaluate RF-EMF-induced heating in a cochlear implant system within a 1.5T MRI coil. The method facilitates the assessment of heating effects on the cochlear implant system and investigates the key factors influencing these thermal effects.

2 MATERIALS AND METHODS

2.1 Cochlear implants

The contemporary generation of cochlear implants consists of two principal components: the implant and an external sound processor. The electrode array in modern cochlear implants typically contains 12 to 22 electrodes, although the exact

number may vary depending on device design and specific clinical requirements. This array, approximately 2 cm in length, is connected to one or more internal current sources, which are activated based on commands from the external device (Macherey & Carlyon, 2014). The external sound processor, worn behind the ear, is removable and can be detached during magnetic resonance imaging (MRI) examinations. As a result, this study focuses exclusively on the radiofrequency electromagnetic field RF-induced heating of the implant portion.

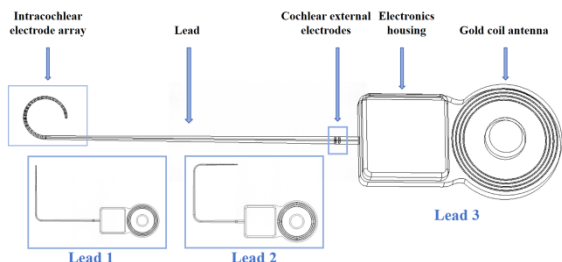


Figure 1: Representative configurations of cochlear implant.

As illustrated in Figure 1, a typical cochlear implant designed by Nurotron comprises consists of several key components, including the intracochlear electrode array, lead, extracochlear electrodes, electronic housing, and gold coil antenna. The intracochlear electrode array is depicted as a 24-electrode cylinder with radii of 0.4 mm, 0.5 mm, and 0.6 mm, respectively, tapering towards the tip of the lead. To accommodate the anatomical variation of the patient’s cochlea and case-specific requirements, the length of the electrode array can be selected from 17.5 mm, 22.0 mm, or 25.5 mm. Additionally, two extracochlear electrodes are also implemented in the system.

2.2 Phantom for Cochlear Implants

The ASTM phantom was used in place of the human body for the simulation. Since the cochlear implant is typically implanted in the human cochlea, and the main components of the cochlear environment include the cochlear canal as well as internal and external lymphatic fluids (Fatani et al., 2024), a configuration simulating the cochlear environment was incorporated. The specific parameters of this configuration are presented in Table 1 (Hasgall PA, 2024), where ϵ_r is the relative dielectric constant, σ (unit: S/m) is the conductivity, k (unit: W/(m²·K)) is the coefficient of thermal

conductivity, c (unit: J/(kg·K)) is the heat capacity, ρ (unit: kg/m³) is the density.

Table 1: Material parameters.

Phantom	ϵ_r	σ	k	c	ρ
ASTM phantom	80	0.47	0.57	4150	1050
Cochlear phantom	57.75	0.32	0.46	3226	1089

The location and trajectory of the cochlear implant within the ASTM phantom are illustrated in Figure 2. The implant is positioned at the center of the ASTM phantom, 45 mm from both the top and bottom of the gel, aligned with the aperture direction, and 2 cm from the sidewalls, where a relatively high and evenly distributed electric field exists. Given that RF-induced heating of partially inserted electrodes is closely correlated with clinically relevant trajectories (Islam et al., 2023), and cochlear implantation often involves electrode bending, this paper discusses several typical simplified cochlear bending trajectories.

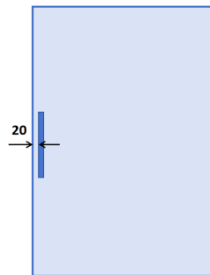


Figure 2: The position and dimension of inserted bone structure. Unit: mm.

2.3 Coupled EM and thermal simulations

An 8-rung 1.5T low-pass birdcage coil (diameter: 800 mm, length: 700 mm) was used to generate a circularly polarized electromagnetic field, driven in quadrature mode at 64 MHz. The ASTM phantom with the implant was positioned such that the center of the phantom aligned with the isocenter of the RF coil. To ensure proper electromagnetic isolation and stable tuning, an RF shield was integrated around the exterior of the birdcage coil. Scattering boundary conditions were applied to truncate the computational region, effectively simulating real-world conditions. The initial value of the capacitance was estimated using the Birdcage Builder Software developed by Penn State University (Chin et al., 2002). A

subsequent scanning search was conducted in the vicinity of this value to determine the optimal capacitance, which was approximately 12.3 pF.

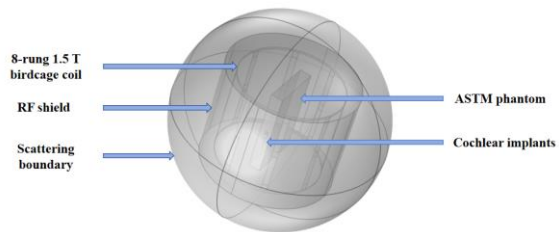


Figure 3: Illustration of simulation setup, the position of various components.

A sequential coupled electromagnetic and thermal analysis was performed using the Finite Element Method (FEM) simulation software COMSOL Multiphysics to calculate the electric and temperature fields for the ASTM phantom cochlear implant model. Maxwell's equations were employed to solve the fluctuating electromagnetic fields at specific points within the model, influenced by the electromagnetic field under investigation, in the steady-state frequency domain. The steady-state electromagnetic solution of Maxwell's equations provided the heat source for the transient thermal analysis, which yielded the electromagnetic solution for all domains and the heat transfer solution within the ASTM body model and the implant. Using the SAR as the heat source for the temperature rise, the temperature field distribution within the model is obtained by solving the heat conduction equation through the Finite Element Method (FEM), as shown in Eq. (1), where ρ is the density of the phantom, c is the specific heat capacity of the phantom, k is the thermal diffusivity, T is the temperature at a point in space, t is time and Q is the heat source.

$$\rho c \frac{\partial T}{\partial t} = k \nabla^2 T + Q = k \nabla^2 T + SAR \quad (1)$$

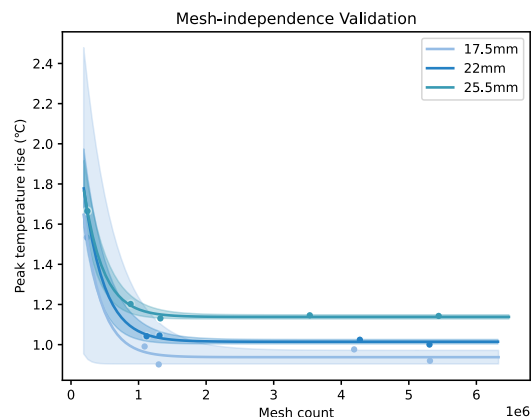


Figure 4: Illustration of mesh-independence validation.

A non-uniform mesh was utilized in the simulation, with the mesh density near critical inflection points selected as the final simulation mesh based on mesh-independence validation. This approach reduced computational costs while maintaining accurate modelling.

3 RESULTS AND DISCUSSION

All results were obtained through numerical simulations using the methodology described above, with the input power of RF coil normalized to a whole-body average SAR of 2 W/kg, in accordance with the IEC 60601-2-33 power limitation criterion for the MR normal mode of operation (Commission, 2022). This study evaluates RF-induced heating in two phantoms with three different electrode lengths and three typical simplified cochlear implant bending trajectory scenarios. This study will analyze the RF-induced heating by examining the spatial and temporal distribution and variation of temperature. It will focus on potential factors affecting maximum temperature rise, including electrode length, lead trajectory, and phantom models.

Table 2: Statistical analysis of temperature rises in phantom around the lead tip under all the studied exposure conditions. (Unit: °C)

(a) ASTM phantom

Bending trajectories	17.5mm electrode length	22mm electrode length	25.5mm electrode length
Lead 1	1.458	1.459	1.461
Lead 2	1.589	1.629	1.746
Lead 3	1.592	1.592	1.597

(b) cochlear phantom

Bending trajectories	17.5mm electrode length	22mm electrode length	25.5mm electrode length
Lead 1	1.456	1.479	1.518
Lead 2	1.736	1.793	1.898
Lead 3	1.906	1.921	1.922

The statistical results of all simulations are presented in Table 2. In the ASTM phantom, the maximum temperature rises for Lead 1, Lead 2, and Lead 3 were 1.461°C, 1.746°C, and 1.594°C, respectively. A similar trend was observed in the cochlear model, where the maximum temperature rises were 1.518°C, 1.898°C, and 1.956°C for Lead 1, Lead 2, and Lead 3, respectively. For a given trajectory, the maximum temperature rise was consistently higher in the cochlear phantom compared to the ASTM phantom.

3.1 Temperature rise distribution

By analyzing the spatial distribution of temperature rise, based on the model's exposure to RF electromagnetic fields for 15 minutes, as shown in Fig. 5, it can be concluded that in several scenarios examined in this study, the areas with the highest temperature increases are concentrated at the ends of the gold coil, the outer cochlear electrode, and the tip of the inner cochlear electrode. The hotspot is primarily located at the tip of the inner cochlear electrode, which warrants focused attention in further research. Theoretically, the implant can be considered an RF antenna that captures energy along its length and dissipates the maximum energy density near its end (Pozar, 2021), which aligns with the observed hotspot at the tip of the intracochlear electrode.

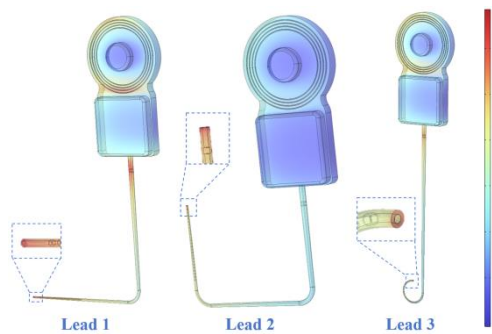


Figure 5: Distribution of temperature rise around the implant after 15 minutes of exposure.

In the time domain, the temperature rise curve shown in Fig. 6 exhibits a rapid, near-linear increase, followed by a gradual leveling off. The rate of

temperature change over time depends on the balance between the power density absorbed from the RF source and heat conduction within the phantom material. As the temperature rise becomes significant, heat conduction begins transferring heat from the implant to the surrounding material, which slows the rate of further temperature increase.

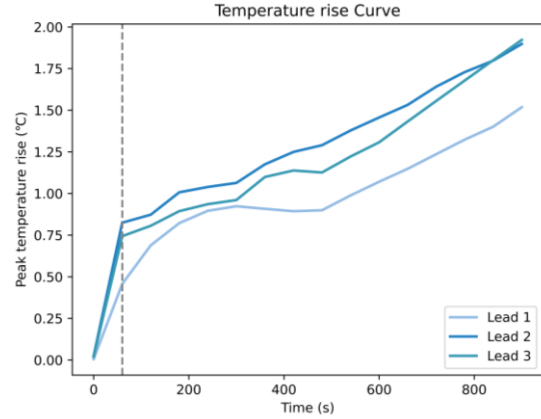


Figure 6: Temperature rise curves for the maximum temperature rise case for three bending trajectories.

3.2 Electrode length

Temperature rises were calculated for three electrode lengths in both ASTM and cochlear phantoms to investigate the effect of electrode length on RF-induced heating. The electrode lengths, chosen based on recommendations from implant surgeons, were 17.5 mm, 22.0 mm, and 25.5 mm to accommodate different cochlear anatomical structures and case variations. The type and number of electrodes remained consistent across lengths, with the primary difference being the spacing between electrodes. The mean RF-induced temperature rises for electrode lengths of 17.5 mm, 22.0 mm, and 25.5 mm were 1.546°C, 1.560°C, and 1.600°C in the ASTM phantom, and 1.699°C, 1.743°C, and 1.779°C in the cochlear phantom. As illustrated in Figure 7(a), the maximum temperature rise tended to increase with longer electrode lengths in both phantoms.

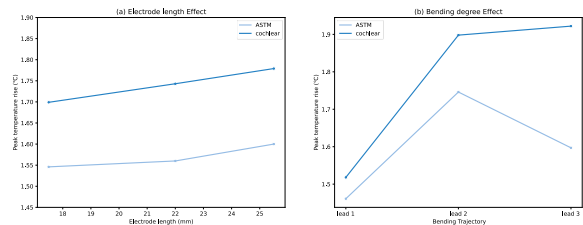


Figure 7: (a) Line graph showing the average maximum temperature rise for different electrode lengths in both the ASTM and cochlear phantoms, (b) line graph showing the

maximum temperature rise for different bending trajectories in both the ASTM and cochlear phantoms.

When the implant's size is approximately half the wavelength, a significant temperature rise occurs due to the resonance effect (Konings et al., 2000). This resonance phenomenon is heavily influenced by the electrical properties and the operating frequency of the medium surrounding the implant. Neglecting magnetic permeability, the wavelength of an electromagnetic wave λ_m in a given material can be calculated using Eq. (2), where λ_0 is the wavelength of the electromagnetic wave in vacuum and ϵ_r is the relative dielectric constant.

$$\lambda_m = \frac{\lambda_0}{\sqrt{\epsilon_r}} \quad (2)$$

The wavelength of an electromagnetic wave in a vacuum λ_0 is related to the RF frequency. In this study, the research focuses on the 1.5T case. According to Eq. (3), the wavelength can be calculated as approximately 4.6875m.

$$\lambda_0 = \frac{c}{f} \quad (3)$$

The relative permittivity of the ASTM phantom is 80, while that of the cochlear phantom is 57.75. Using these values and applying Eq. (2), the theoretical half-wavelengths are calculated as 26.20 and 30.84mm, respectively, for ASTM and cochlear phantom. The cochlear implant leads tested thus far have not reached this length, so, theoretically, the temperature rise is expected to increase as the lead length increases. The conclusion that the maximum temperature rise increases with longer electrode length aligns with theoretical expectations.

3.3 Bending Trajectory

Cochlear implantation often involves lead bending, and three typical simplified bending trajectories, as shown in Fig. 1, were investigated for both the ASTM and cochlear phantoms. Figure 7(b) illustrates the surrounding temperature rise for different implantation trajectories in the two phantoms, with maximum temperature rises of 1.518°C, 1.898°C, and 1.922°C for trajectories 1, 2, and 3, respectively. It can be tentatively estimated that trajectories with a greater degree of curvature and a smaller bending range will concentrate more heat and cause a larger temperature rise.

3.4 Phantom Model

The RF-induced thermogenesis of the same implant differs between the ASTM and cochlear phantoms. Table 2 and Figure 7 presents histograms of the maximum temperature rise in both phantoms, showing that the mean maximum temperature rise in the ASTM phantom is 1.569°C, which is lower than the 1.737°C observed in the cochlear phantom. In all cases, the maximum temperature rise in the ASTM phantom is lower than that in the cochlear phantom. Similar to Yang et al.'s study, relying solely on the ASTM phantom for localized areas may result in temperature rise deviations (Yang et al., 2024). In this paper, it is shown as an underestimation of the maximum temperature rise. Therefore, when assessing the RF thermogenic safety of cochlear implants more localized scenarios should be considered.

4 CONCLUSIONS

In this study, we introduce a model that simulates the cochlear environment to improve the assessment of RF-induced heating near cochlear implants. This model provides results that more accurately reflect the intracochlear conditions compared to the ASTM model, verifying that the ASTM model may have underestimated the maximum temperature rise. Additionally, we propose a finite element-based electromagnetic and thermal co-simulation method to obtain the temperature distribution and maximum temperature rise from RF thermogenesis. This approach enables rapid analysis of worst-case implant configurations and predicts RF thermogenesis outcomes, helping to guide future experiments and implant design. Using this method, we examine factors such as electrode length and wire trajectory, highlighting the importance of focusing on the hotspot at the tip of the electrode and emphasizing the need to control electrode length where possible.

ACKNOWLEDGEMENTS

This research was supported by the Key Research and Development Plan of Zhejiang Province (Grant Nos. 2023C03094) and Zhejiang Provincial Natural Science Foundation of China under Grant No. LY22H180006.

REFERENCES

- Alberalar, N. D., Reis, J., Piechotta, P. L., Beetz, N. L., Fehrenbach, U., Geisel, D., Thomas, A., Busse, H., & Denecke, T. (2023). Complications of cochlear implants with MRI scans in different body regions: type, frequency and impact. *Insights into imaging*, 14(1), 9. <https://doi.org/10.1186/s13244-022-01353-x>
- ASTM_International. (2019). Standard Test Method for Measurement of Radio Frequency Induced Heating On or Near Passive Implants During Magnetic Resonance Imaging(F2182 - 19e2).
- Buchman, C. A., Gifford, R. H., Haynes, D. S., Lenarz, T., O'Donoghue, G., . . . Zwolan, T. (2020). Unilateral Cochlear Implants for Severe, Profound, or Moderate Sloping to Profound Bilateral Sensorineural Hearing Loss: A Systematic Review and Consensus Statements. *JAMA Otolaryngol Head Neck Surg*, 146(10), 942-953. <https://doi.org/10.1001/jamaoto.2020.0998>
- Chadha, S., Kamenov, K., & Cieza, A. (2021). The world report on hearing, 2021. *Bull World Health Organ*, 99(4), 242-242a. <https://doi.org/10.2471/blt.21.285643>
- Chin, C. L., Collins, C. M., Li, S., Dardzinski, B. J., & Smith, M. B. (2002). BirdcageBuilder: Design of Specified-Geometry Birdcage Coils with Desired Current Pattern and Resonant Frequency. *Concepts Magn Reson*, 15(2), 156-163. <https://doi.org/10.1002/cmr.10030>
- Commission, I. E. (2022). Particular requirements for the basic safety and essential performance of magnetic resonance equipment for medical diagnosis.(IEC 60601-2-33 ED4.0).
- Crane, B. T., Gottschalk, B., Kraut, M., Aygun, N., & Niparko, J. K. (2010). Magnetic resonance imaging at 1.5 T after cochlear implantation. *Otol Neurotol*, 31(8), 1215-1220. <https://doi.org/10.1097/MAO.0b013e3181ec1d61>
- Fatani, N., Abdelsamad, Y., & Alsanosi, A. (2024). Influence of Cochlear Anatomy on Intraoperative Electrically Evoked Compound Action Potentials. *J Clin Med*, 13(16). <https://doi.org/10.3390/jcm13164716>
- Hasgall PA, D. G. F., Baumgartner C, Neufeld E, Lloyd B, Gosselin MC, Payne D, Klindingböck A and Kuster N. (2024). *IT'IS Database for Thermal and Electromagnetic Parameters of Biological Tissues, Version 4.2*. <https://doi.org/10.13099/VIP21000-04-2>.
- Islam, M. Z., Hu, W., Guo, R., & Chen, J. (2023). *Factors Affecting the RF-Induced Heating for the Electrodes Partially Inserted Inside Human Body at 1.5T MRI* 2023 IEEE International Symposium on Antennas and Propagation and USNC-URSI Radio Science Meeting (USNC-URSI).
- Konings, M. K., Bartels, L. W., Smits, H. F., & Bakker, C. J. (2000). Heating around intravascular guidewires by resonating RF waves. *Journal of Magnetic Resonance Imaging*, 12(1), 79-85.
- Koptyug, I., Kovtunov, K., & Svyatova, A. (2023). Magnetic Resonance Imaging (MRI). In I. E. Wachs & M. A. Bañares (Eds.), *Springer Handbook of Advanced Catalyst Characterization* (pp. 849-867). Springer International Publishing. https://doi.org/10.1007/978-3-031-07125-6_37
- Luechinger, R., Zeijlemaker, V. A., Pedersen, E. M., Mortensen, P., Falk, E., . . . Boesiger, P. (2005). In vivo heating of pacemaker leads during magnetic resonance imaging. *Eur Heart J*, 26(4), 376-383; discussion 325-377. <https://doi.org/10.1093/eurheartj/ehi009>
- Macherey, O., & Carlyon, R. P. (2014). Cochlear implants. *Current Biology*, 24(18), R878-R884. <https://doi.org/10.1016/j.cub.2014.06.053>
- Pozar, D. M. (2021). *Microwave engineering: theory and techniques*. John Wiley & sons.
- Ran, G., Jianfeng, Z., & Ji, C. (2017). MRI RF-Induced Heating in Heterogeneous Human Body with Implantable Medical Device. In H. Ahmet Mesur (Ed.), *High-Resolution Neuroimaging*. IntechOpen. <https://doi.org/10.5772/intechopen.71384>
- Rezai, A. R., Finelli, D., Nyenhuis, J. A., Hrdlicka, G., Tkach, J., . . . Shellock, F. G. (2002). Neurostimulation systems for deep brain stimulation: in vitro evaluation of magnetic resonance imaging-related heating at 1.5 tesla. *J Magn Reson Imaging*, 15(3), 241-250. <https://doi.org/10.1002/jmri.10069>

- Standardization, I. O. f. (2018). Assessment of the safety of magnetic resonance imaging for patients with an active implantable medical device(Tech Specif ISOTS 10974 2018, second edition).
- Winter, L., Seifert, F., Zilberti, L., Murbach, M., & Ittermann, B. (2021). MRI-Related Heating of Implants and Devices: A Review. *J Magn Reson Imaging*, 53(6), 1646-1665. <https://doi.org/10.1002/jmri.27194>
- Yang, X., Guo, R., Zheng, J., Long, S. A., Chen, X., & Chen, J. (2024). Improved assessment of radiofrequency electromagnetic field power deposition near orthopaedic device using a bone-inclusive ASTM phantom under 1.5 T and 3T MRI. *Physics in Medicine & Biology*, 69(16), 165024.
- Zeng, Q., Wang, Q., Zheng, J., Kainz, W., & Chen, J. (2018). Evaluation of MRI RF electromagnetic field induced heating near leads of cochlear implants. *Phys Med Biol*, 63(13), 135020. <https://doi.org/10.1088/1361-6560/aacbf2>